A Model for In-Process Control of Thermal Properties During Welding

C. C. Doumanidis
Research Assistant.

D. E. Hardt
Associate Professor.

Laboratory for Manufacturing and Productivity,
Massachusetts Institute of Technology,
Cambridge, MA 02139

The control of welding processes has received much attention in the past decade, with most attention placed on real-time tracking of weld seams. The actual process control has been investigated primarily in the context of weld bead geometry regulation, ignoring for the most part the metallurgical properties of the weld. This paper addresses the latter problem through development of a model for in-process control of thermally activated material properties of weld. In particular, a causal model relating accessible inputs to the outputs of weld bead area, heat affected zone width, and centerline cooling rate at a critical temperature is developed. Since the thermal system is a distributed parameter, nonlinear one, it is modelled numerically to provide a baseline of simulation information. Experiments are performed that measure the thermal response of actual weldments and are used to calibrate the simulation and then to verify the basic dynamics predicted. Simulation results are then used to derive a locally linear transfer function matrix relating inputs and outputs. These are shown to be nonstationary, depending strongly upon the operating point and the boundary conditions.

1 Introduction

Weld quality factors usually encompass static and dynamic loading capacity, fracture toughness, oxidation and corrosion resistance, geometric tolerances of the joint, or even functionality and aesthetics of the bead form, with the specific importance of each feature depending on the particular application. Thus an in-process weld quality control system would typically need to regulate in a multivariable fashion several weld characteristics simultaneously. These can be grouped as:

(a) Weld bead location relative to the seam;
(b) Weld bead geometry, typically characterized by the bead width, penetration, and reinforcement height;
(c) Thermally induced stress-strain effects, resulting in residual stresses and distortion of the joint;
(d) Material microstructure, the alteration of which during welding affects the final material properties.

Because of the complexity of the overall control problem and the lack of comprehensive specifications, the control systems developed so far deal with characteristics of a single type (or more commonly a single variable within these groups) only, and the above groups reflect the attention that each of them has received in the related literature. The lion's share of the recent research efforts has been expended in the seam tracking problem, with a moderate effort being devoted to the bead geometry control, and to a minor extent the control of residual stresses and distortion [1-6]. The effects of the fusion welding process on the material structure and the final mechanical properties have been neglected so far by all control schemes, in spite of their obvious influence on the weld quality, particularly in cases involving extensive solidification defects, sensitization zones or martensitic weld beads [7-9]. It is the objective of this paper to address this latter problem and to develop a dynamic model of some thermally activated properties of weldments that define the final microstructure distribution and thus the final material properties of the weld. In a subsequent paper, the use of this model in a nonlinear, multivariable control system will be detailed.

The block diagram of Fig. 1(a) illustrates the dependence of these properties on the welding process. The welding inputs, i.e., the settings of the welding machine, are selected so that, during the process, the temperature field history defines the final microstructure through the various metallurgical mechanisms and thus determines the material properties of the weld. This open-loop control scheme by its very nature is vulnerable to various disturbances and susceptible to significant process modeling uncertainties. These include geometry changes (caused by thickness and groove shape variations, and by tack welds), material properties (in particular the thermal diffusivity), thermal boundary conditions (such as preheat, and variable thermal resistance of heat sinks), and arc process changes (such as efficiency, heat distribution and pool convection).

However, if closed-loop control is to be adopted, it is impractical to use feedback of final microstructure or material property related quantities because of the large transportation lags involved and because equipment for in-process sensing of these is not well developed. Rather, it is possible to employ measurable temperature field characteristics for feedback and still use open-loop control of the final microstructure and resulting material properties, as in Fig. 1(b). This is not overly restrictive, since most modeling uncertainties are related to, and most disturbances occur during, the welding process itself. In this configuration the temperature measurements are used to estimate a set of welding outputs that describe the final

Contributed by the Dynamic Systems and Control Division for publication in the JOURNAL OF DYNAMIC SYSTEMS, MEASUREMENT, AND CONTROL. Manuscript received by the Dynamic Systems and Control Division August 11, 1987.

microstructure and material properties, since the latter depend nearly deterministically on thermal history [10, 11]. These welding outputs can in turn be regulated to some specified (or reference) values in order to ensure the desired weld quality.

This paper concentrates on definition of appropriate outputs and inputs of the welding process and development of a dynamic model for use in control system design. The selection of the welding inputs and outputs is predicated upon the availability of output measurements (observability in the I/O sense), the efficient modulation of the outputs by the inputs (controllability in the I/O sense), and, if possible, the selection of independent input-output pairs (decoupledness). Although the fundamental dynamic model will be a nonlinear, distributed parameter model, it will be shown that it can be approximated by a linear, lumped parameter model, i.e., linearized within an appropriate operating range, because of the intended structure of the multivariable closed-loop control system. A brief discussion of this latter topic will be presented at the end of the paper.

2 Selection of the Welding Outputs

As already mentioned, the welding outputs derived from a (topside) temperature field must be chosen so as to characterize the resulting microstructure and material properties as accurately as possible. The relationship between temperature history and resulting metallurgy was extensively reviewed [10, 11] for most commonly welded materials, ranging from plain carbon steels to titanium alloys, in an attempt to identify classes of common metallurgical mechanisms activated in these materials during welding, and thus common potential problems affecting the final microstructure and material properties. The following selection of welding outputs was suggested by this review:

(*a*) *The weld nugget cross section area NS*, defined by the solidus isotherm T_m. This is adopted as a collective measure of the extent of solidification defects [11], such as porosity, inclusions, incomplete fusion, micro-cracks, columnar structure, uneven grain size, micro-segregation and nucleation of undesirable phases. It also characterizes the dilution of the base material with filler material, when a consumable electrode or filler rod is used. Finally, it also provides for eventual coupling of this model with a similar bead geometry control model [12].

(*b*) *The heat affected zone width HZ*, defined by an enveloping isotherm T_h. This may indicate the extent of weak zones, such as the recovery, recrystallization and grain growth areas, or the width of the zone in which some undesirable, thermodynamically favored phase is formed, such as the sensitization zone in stainless steels (Cr_4C). It may also characterize the extent of the contamination zone in cases of increased reactivity of the material with its environment during welding, such as titanium and its alloys.

(*c*) *The centerline cooling rate CR*, defined at the critical temperature T_c. This may determine the crystallization of undesirable, kinetically favored phases, such as the martensite in high-carbon steels, or supply a measure of the cracking tendency of the weldment caused by thermal stresses.

The definition of the welding outputs is given in Fig. 2. Note that NS is currently defined assuming transverse symmetry of the pool; HZ is measured from the edge of the weld bead and CR is dynamically defined in the Lagrangian sense. It is clear that for each of the above welding outputs the correlation to particular attributes of the final microstructure and material properties, as well as its importance to the overall weld quality, depends on the specific material. As an example, in welding a titanium α-alloy, the cross section of the bead NS would indicate the extent of the zone in which brittle intermetallic compounds are formed and solution strengthening or freezing segregation occur. The heat affected zone width HZ would need to be controlled in order to limit the contamination-increased reactivity area enveloped by the 1200°F isotherm, while the regulation of the centerline cooling rate CR would ensure the complete transformation β- to α-phase. A detailed account of these effects for a wide range of engineering metals is presented in [10].

3 Selection of Welding Inputs

Having identified the welding outputs NS, HZ, and CR, the selection of controllable quantities that exert an important and decoupled effect on the outputs and thus can serve as the welding inputs is now in order. Insight as to the nature of the dependence of the selected outputs to prospective inputs was provided by a comprehensive review of the temperature field models in the literature [10], typically classified as:

(*a*) Analytical models [13–31]
(*b*) Empirical models [32–41]
(*c*) Numerical models [42–51].

Although no single existing model offers satisfactory input-output dynamic dependencies for in-process control purposes, the classical (or Rosenthal) steady-state thermal conduction model provides a useful tool in assessing the sensitivity and decoupledness of the selected outputs on various inputs [13, 15, 17]. The temperaure field developed by either a line or point source can be solved for the maximum width of the T_m and T_h isotherms and the centerline cooling rate at T_c, yielding the following expressions of the welding outputs as functions of the heat input Q, torch velocity v and preheat temperature T_0:

$$\mathrm{NS} = c_1 \left(\frac{Q}{v^g}\right)^{n_a} \left(\frac{1}{T_m - T_0}\right)^{n_q} \qquad (1a)$$

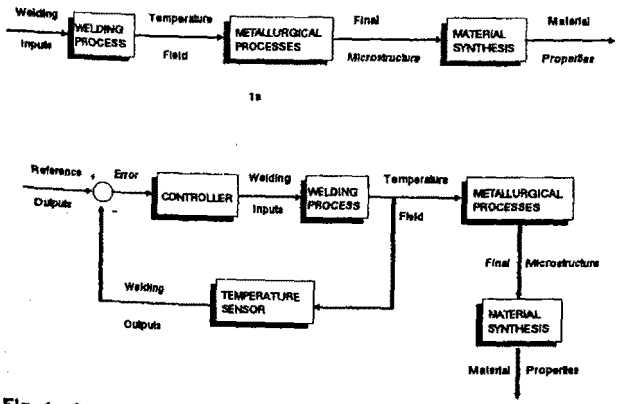

Fig. 1 Schematic causality of the welding process: (*a*) Open-loop, (*b*) Closed-loop

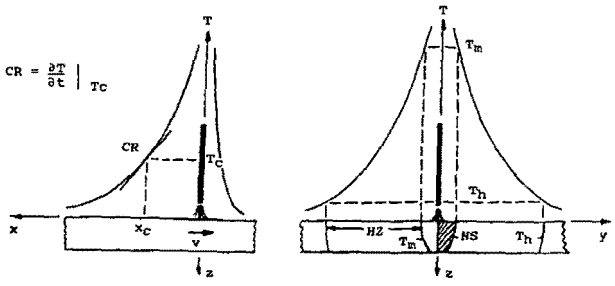

Fig. 2 Definition of the welding outputs NS, HZ, CR

$$HZ = c_2\left(\frac{Q}{v^f}\right)^{1/n_b}\left[\left(\frac{1}{T_h - T_0}\right)^{1/n_b} - \left(\frac{1}{T_m - T_0}\right)^{1/n_b}\right] \quad (1b)$$

$$CR = c_3\left(\frac{Q}{v}\right)^{-n_c}\left(\frac{1}{T_c - T_0}\right)^{-(n_c+1)} \quad (1c)$$

where $f = n_b - (n_b - n_2)/(n_3 - n_2) \approx 1$, $g \approx 2/3$ and the conduction exponents $n_2 = 0.96$, $n_3 = 1.70$ (see [24] for complete derivation). The coefficients c_1, c_2, c_3 and the exponents n_a, n_b, n_c depend on the geometry and material of the plates as well as on the specific process and environmental conditions, and they are evaluated in [10] on the basis of conduction theory.

From equations (1*a*, *b*, *c*) it is clear that the heat input Q and torch velocity v are suitable as welding inputs, but the use of the preheat temperature T_0 as a direct control input (which could be implemented by a leading preheat torch) is associated with a number of problems, such as nonuniformity and transportation lags. Note, however, that although in the above relationships the dependence of NS and HZ on the overtemperatures $(T_h - T_0)$ and $(T_m - T_0)$ is at the same exponent as the heat input Q, there is a difference of 1 in the respective exponents of $(T_c - T_0)$ and Q in the expression for CR. Thus it was decided to exploit this selective dependence of the cooling rate on the preheat temperature T_0, and to take advantage of the preheating effect of the main torch itself by employing a trailing secondary torch, following at a fixed distance (Fig. 3). As illustrated in this figure, the heat input of the secondary torch Q_2 can be restricted in a range ensuring that the bead cross section and the heat affected zone generated by the secondary torch do not exceed the magnitudes of those of the primary torch, thus NS and HZ are exclusively determined by the main torch characteristics (heat input Q_1). However, because of the selectivity of the preheating effect on the cooling rate, the cooling rate can be independently modulated in the same range of values of Q_2, which thus exerts a decoupled effect on CR without affecting NS or HZ. Using hindsight, one can think of the use of a secondary torch as an in-process implementation of a post-heating cycle or as the reshaping of the temperature field by using an additional source.

To determine the control range of the cooling rate by the secondary torch, an optimization problem was solved in [10], on the basis of the steady-state conduction model for both a line and a point source. This determined the optimum values of the secondary torch distance x and heat input Q_2 for which the absolute value of the cooling rate CR is minimized without affecting the other outputs NS and HZ, and the maximum obtainable reduction of |CR| was found to be 25–38.5 percent for the double torch configuration. If a larger control range is desired for CR, a multiple torch configuration can be employed, and again an optimization problem for N distinct torches determined that |CR| can be reduced by 50–100 percent as $N \to \infty$, without affecting NS and HZ.

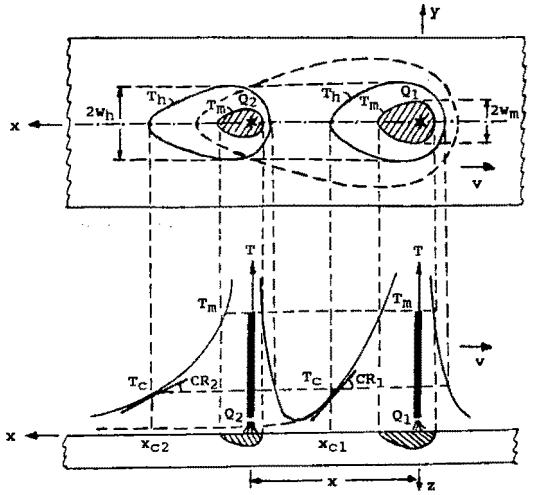

Fig. 3 The double-torch welding configuration

For acutal implementation, multiple torches have the disadvantages of multiple power supplies and possible electromagnetic interference. However, a timesharing of the heat source, whereby the mean torch velocity is held constant while high frequency longitudinal velocity variations occur to alter the heat input distribution, can be accomplished since the characteristic time constant of the arc is orders of magnitude shorter than that of weldment heat transfer. Such motion can be imposed either with modification to the torch manipulator path or by magnetic deflection of the arc [39]. This allows the possibility of a continuous heat distribution modulation along the weld line, effectively mimicking infinite torch case.

4 Double-Torch Steady-State Model

If the configuration is confined to the use of a single secondary torch, then the temperature fields of the two torches can be superimposed, because of the linearity of the conduction equation for invariant material properties, and the composite field for the input-output relationships can be solved as before. These can be combined with empirical (i.e., experimentally derived) relationships in the literature [34, 37, 38, 41] by introducing appropriate correction factors. Thus the following steady-state model can be derived for the double-torch configuration:

$$NS = C_1\left(\frac{Q_1}{v^g}\right)^{n_a}$$

$$HZ = C_2\left(\frac{Q_1}{v^f}\right)^{1/n_b} \quad (2)$$

$$CR = C_3\left(\frac{Q_1}{v}\right)^{-n_c}\left(1 - \beta\frac{Q_2}{Q_1}\right)$$

which relates the welding outputs NS, HZ, CR to the welding inputs Q_1, v and Q_2. The coefficients C_1, C_2, C_3, and β and the exponents n_a, n_b, and n_c can be determined in-process by system identification procedures presented in [10]. The form of the above steady-state model description gives a first indication of the highly nonlinear nature of the fusion welding process.

5 Nonlinear Dynamic Model

The modeling of the dynamic dependence of the welding outputs on the inputs involves resorting to the transient conduction model, which is based on the integration of an appropriate Green's function [10, 13]. A solution of the respective time-dependent temperature field for the dynamic input-output relationships turned out to be impractical and limited in scope, since it could not cope with the three-dimensional welding geometry, the phase transformations and temperature dependence of the material properties, the complexity of the initial and ambient conditions and the diversity of the welding process characteristics. In order to handle these effects, a versatile and general-purpose numerical simulation of the temperature field for the multi-torch welding configuration was developed. The simulation program integrates the unsteady conduction (Fourier) equation:

$$\frac{\partial T}{\partial t} = \alpha\nabla^2 T \quad (3)$$

where T is the temperature and α the thermal diffusivity of the material. This is done in discrete time steps Δt and space elements Δs by employing an explicit Euler finite difference formulation:

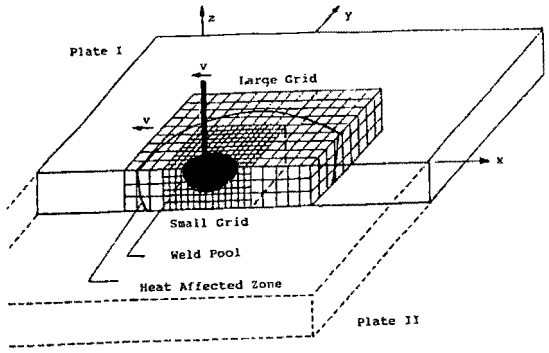

Fig. 4 The geometrical arrangement of the numerical simulation

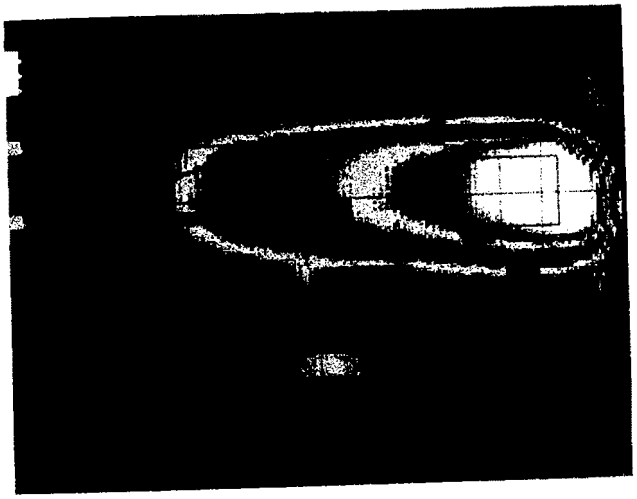

Fig. 5 Top surface temperature field at the nominal conditions

$$T(t+\Delta t)=T(t)+\frac{\alpha\Delta t}{\Delta s^2}\left(\sum_{i=1}^{6}T_i(t)\Big|_{\Delta s}-6T(t)\right), \quad (4)$$

where $T(t)$ is the temperature at time t and $T_i(t)$ the temperature of its neighboring points at distance Δs in the three dimensions. The alternate forms of equation (4) in the presence of conductive, convective and radiative boundary conditions are detailed in [52], along with the simulation program. However, the main features of this model are given below.

The simulation program is based on symmetric butt welding of two plates of finite thickness, and it features a pair of orthogonal grids of nodes moving with the torches (Fig. 4). The external coarse grid encompasses the enveloping isotherm T_h of the HAZ while the internal fine grid encompasses the weld pool isotherm T_m for more accuracy. An arbitrary number of torches are arranged along the weld centerline at arbitrary distances.

The time histories of the heat inputs and speed of torches are arbitrary in order to be able to simulate realistic control action. The spatial distribution of the heat inputs is also arbitrary, permitting both distinct multitorch and continuous distribution configurations, with the default being a centrally symmetric elliptic Gaussian distribution for each torch, with selectable distribution radii [52].

The initial temperature field is arbitrary and is typically defined by a uniform preheat temperature T_o. The boundary conditions provide for convective and radiative heat losses from the two surfaces of the plates.

There is provision for an arbitrary temperature dependence of the material properties and for latent fusion-solidification effects during welding. The convective heat transfer in the weld pool is accounted for by directional equivalent conduction factors determined experimentally and reported in the literature [52, 53].

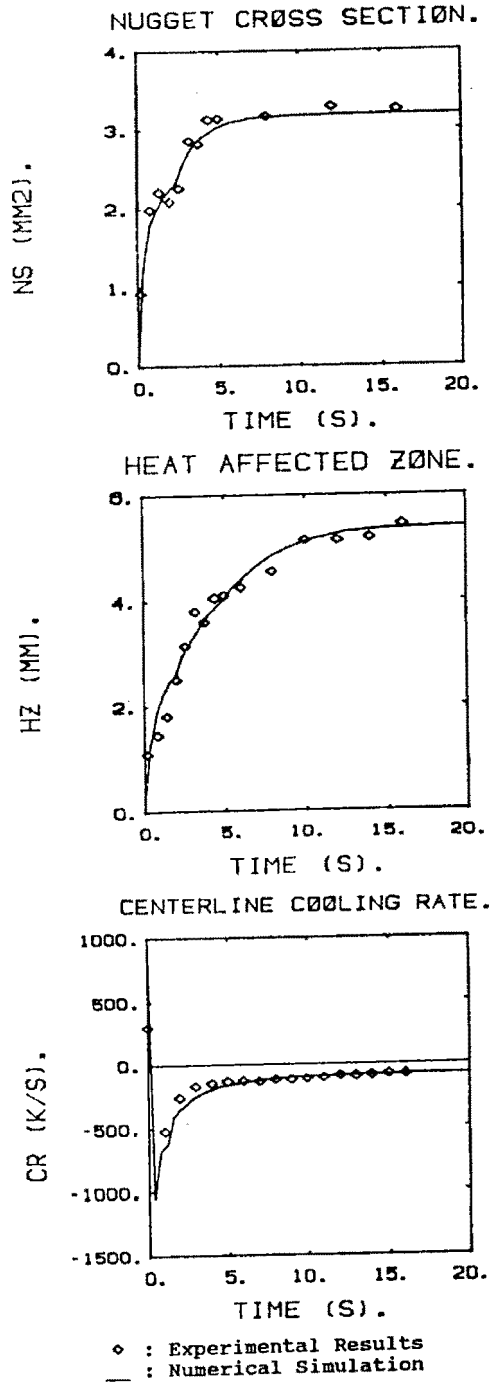

Fig. 6 Time responses of the output during the transient to the nominal conditions ($Q_1^* = 2500$ W, $v^* = 5$ mm/s, $Q_2^* = 0$ W)

The output is in the form of temperature and phase distribution contours at arbitrary sections of the plates, as well as sections and 3D plots of the temperature hills and isotherm surfaces. The cross section of the zone in which the cooling rate has exceeded a critical value CR_{max} at the temperature T_c is also given, together, of course, with the time histories of the welding outputs NS, HZ, and CR.

The numerical model requires experimental calibration of a number of parameters, namely the arc efficiencies of the torches, the heat input distribution radii and the equivalent conduction factors in the melt. The rest of the necessary calorimetric data regarding the heat transfer to the environ-

ment as well as the material thermal properties and their temperature dependence were taken from the literature [27, 46, 52–56].

6 Experimental Calibration of the Model

The experiments performed consisted of single torch Gas Metal Arc (GMA) butt welding of thin mild steel plates, with 1/8 in thickness. The wire feed and gas (A) flow were constant, and no preheat was used. The welding inputs were conveniently modulated through the software of the welding robot [57], i.e., by controlling in closed-loop the torch speed v and the arc voltage V, so that the product VI provided the necessary heat input Q_1. The heat affected zone was enveloped by an assumed recrystallization isotherm $T_h = 824$ K, and the cooling rate was measured at the austenitization temperature $T_c = 996$ K.

The on-line thermal measurements consisted of scanning the time-dependent temperature field on the top and bottom surface of the plates using an infrared radiation camera system [58], sensitive in the range of 8–14 μm (HgCdTe detector, liquid nitrogen cooled). The mechanical scanner was stationary relative to the welded pieces, with its horizontal axis parallel to the weld centerline, at a distance of 0.8 m and a viewing angle of 30 deg relative to the plane of welding. The resulting field of view was 300×40 mm, with a spatial resolution of 1.2×0.2 mm and the dynamic temperature range varied between 400–1400 K, with an accuracy of ± 2 K for a given emmissivity ϵ. The infrared pyrometry images were stored using standard video format (30 Hz) and analyzed off-line using a thermal image processor [59] (Fig. 5) to determine the T_h and T_m isotherms and the centerline profiles. Finally the bead geometry was studied by successive transverse sectioning, Nital etching, and microscopic observation of the bead cross section.

The experimental calibration of the parameters was performed at a set of inputs producing outputs approximately in the middle of the specified or desirable range (usually limited by unacceptable fusion penetration or lack of fusion and excessive porosity). These "nominal" conditions were:

$Q_1^* = 2500$ W		$NS^* = 3.30$ mm^2
$v^* = 5$ mm/s	corresponding to	$HZ^* = 5.39$ mm
$Q_2^* = 0.0$ W		$CR^* = -82.2$ K/s

Figure 6 presents the experimentally observed values of the outputs during the transient from zero to the nominal conditions, with the solid line representing the response of the simulation to the same set of inputs. The model parameters were calibrated so that this response matches the experimental data in an approximate ITAE sense (yielding an arc efficiency of 0.869, a heat distribution radius of 1.71 mm and an equivalent weld pool conduction factor of 3.57). Note that the infrared pyrometer emmissivity value of 0.69 was also calibrated at the nominal conditions by matching the top surface width of the melting isotherm T_m to the actual weld bead width measured on its cross section. Finally, the impulsive response of the cooling rate at the beginning of welding is further discussed in Section 9.

7 Experimental Assessment of the Welding Dynamics

Having calibrated the dynamic model, the dynamics of the welding process can now be studied both by experiment and by simulation. This is done by starting at the nominal conditions and obtaining the transient response of the welding system to steps in the inputs Q_1, v, and Q_2. The steps applied to each input go approximately half the way between the nominal conditions and the most extreme values of inputs that the system is expected to handle in practice. The simulations performed are listed below:

#	Step	Input	Initial value	Final value	Fig. #
(a)	Positive step	to Q_1,	from $Q_1^* = 2500$W	to $1.2^* Q_1 = 3000$W	(Fig. 7)
(b)	Negative step	to Q_1,	from $Q_1^* = 2500$W	to $0.8^* Q_1 = 2000$W	(Fig. 8)
(c)	Positive step	to v,	from $v^* = 5$mm/s	to $1.2^* v = 6$mm/s	(Fig. 9)
(d)	Negative step	to v,	from $v^* = 5$mm/s	to $0.8^* v = 4$mm/s	(Fig. 10)
(e)	Positive step	to Q_2,	from $Q_2^* = 0.0$ W	to $Q_{srce} = 250$ W	(Fig. 11)
(f)	Negative step	to Q_2,	from $Q_2 = 0.0$ W	to $Q_{sink} = -250$W	(Fig. 12)

Thus, for example, Fig. 7 presents the measured and calculated output response after a step increase of the heat input Q_1 by 20 percent. The response of the calibrated simulation is indicated by the dashed line, which sometimes is at a small steady-state error with respect to the experimental data. These can be fitted better in an approximate ITAE sense by just a slight adjustment of the calibration parameters, in which case the response of the simulation is shown with the solid line. Finally the dot-dashed line corresponds to the response of a lumped parameter, linearized model, which is discussed later. The same notation is used in Figs. 7–12.

Figure 11 illustrates the responses of the outputs to a positive step applied to the heat input Q_2 of a secondary torch positioned 10 mm behind the main torch. Since an experiment using the second torch was not performed, the predicted responses may include small quantitative inaccuracies as before. Figure 12 shows the analogous responses of the simulation and linearized model for a negative step of equal magnitude in Q_2, provided by a heat sink (such as a cooling shoe or jet) at the same distance behind the main torch as before. These are given for theoretical completeness, since a heat sink is more difficult to implement in practice and it tends to increase (absolutely) the cooling rate, while usually only an upper (absolute) bound is specified on CR. The decoupling between Q_2 and NS and HZ is discussed further in Section 9.

The nonlinear nature of the system is illustrated by the different response to inputs of different magnitude, i.e., the dependence of the above step responses of all the outputs on the value of the step applied to each of the inputs. Indeed, the steady-state deviations of the outputs from the nominal conditions after the transient are markedly different for positive and negative steps of the same size applied to the inputs and there is also an apparent dependence in the settling time. Also, the dynamic dependencies are of higher order, as it is clear from the often irregular and nonsmooth nature of the step responses.

8 Linearized Dynamic Model

While the calibrated simulation can be used as a dynamic model of the welding process, a linear low-order description of the input-output dependencies is more useful as a model during the design of a control system for the welding process. Thus the dynamic model can be linearized in the neighborhood of the nominal conditions for limited ranges of variation of the inputs, and described in terms of low-order transfer functions. The form and parameters of the latter must be selected so that the responses match as closely as possible the previous experimental data (or the nonlinear simulation response in the case of the secondary heat input Q_2). In the following analysis the values of the welding inputs and outputs refer to deviations from the nominal conditions.

The response of the bead cross section area NS to steps in either Q_1 or v can be approximated by the expected [1, 2] overdamped second order behavior, in which one pole clearly

dominates over the other, so that NS may be adequately modelled by a first order transfer function with respect to either Q_1 or v [4]. As it appears in Figs. 11 and 12, NS does not respond to small enough steps of Q_2, i.e., it is decoupled from the effect of the secondary torch (see section 9). Consequently, the proposed transfer functions are of the form:

$$\frac{\text{NS}}{Q_1}(s) = \frac{K_a}{\tau_a s+1},$$
$$\frac{\text{NS}}{v}(s) = \frac{K_a'}{\tau_a' s+1}, \tag{5}$$
$$\frac{\text{NS}}{Q_2}(s) = 0.$$

The response of the heat affected zone width HZ to steps in either Q_1 or v has a nonminimum phase response, the basis for which is discussed in the next section. Accordingly, it can be closely approximated by a nonminimum phase second order behavior of the form:

$$\frac{K_b(\tau_b s+1)}{(\tau_1 s+1)(\tau_2 s+1)} = \frac{K_1}{\tau_1 S+1} - \frac{K_2}{\tau_2 S+1}, \quad \tau_b<0, \tag{6}$$

where the two modes can be associated with the dynamics of the two isotherms T_h and T_m the width difference of which defines HZ. The sensitivity of HZ to the third input Q_2 is almost insignificant, as illustrated in Figs. 11 and 12 by the very small steady-state deviations of HZ from the nominal conditions after a step in Q_2. For the completeness of the model a first order dependence of HZ on Q_2 will be considered here, so that:

$$\frac{\text{HZ}}{Q_1}(s) = \frac{K_b(\tau_b s+1)}{(\tau_1 s+1)(\tau_2 s+1)},$$
$$\frac{\text{HZ}}{v}(s) = \frac{K'_b(\tau'_b s+1)}{(\tau'_1 s+1)(\tau'_2 s+1)}, \tag{7}$$
$$\frac{\text{HZ}}{Q_2}(s) = \frac{K_b''}{\tau_1'' s+1} (\approx 0).$$

Finally the response of the centerline cooling rate CR to steps in either Q_1 or v may be approximately described by an over-damped second order behavior owing to the existence of two dominating real poles. The dependence of CR on the third input Q_2 is also of second order, but with the one pole dominating over the other, so that it can be simplified to a first order transfer function:

$$\frac{\text{CR}}{Q_1}(s) = \frac{K_c}{(\tau_\alpha s+1)(\tau_\beta s+1)},$$
$$\frac{\text{CR}}{v}(s) = \frac{K_c'}{(\tau_\alpha' s+1)(\tau_\beta' s+1)}, \tag{8}$$
$$\frac{\text{CR}}{Q_2}(s) = \frac{K_c''}{\tau_\alpha'' s+1}.$$

Section 9 further elaborates on the dynamics of the cooling rate.

The values of the gains of all the proposed transfer functions are easily determined from the steady-state values of the respective outputs (at $t=0$ and $t=\infty$) and the magnitudes of the steps imposed to the respective inputs. The time constants are calculated by a weighted averaging of those values that make the linearized responses to match (go through) the experimental data (or the simulated response in the case of Q_2) at the corresponding sequence of time instants.. This is done separately for each of the two modes of the heat affected zone width, as well as for those of the cooling rate, where the secondary time constants τ_b are selected to make the second order

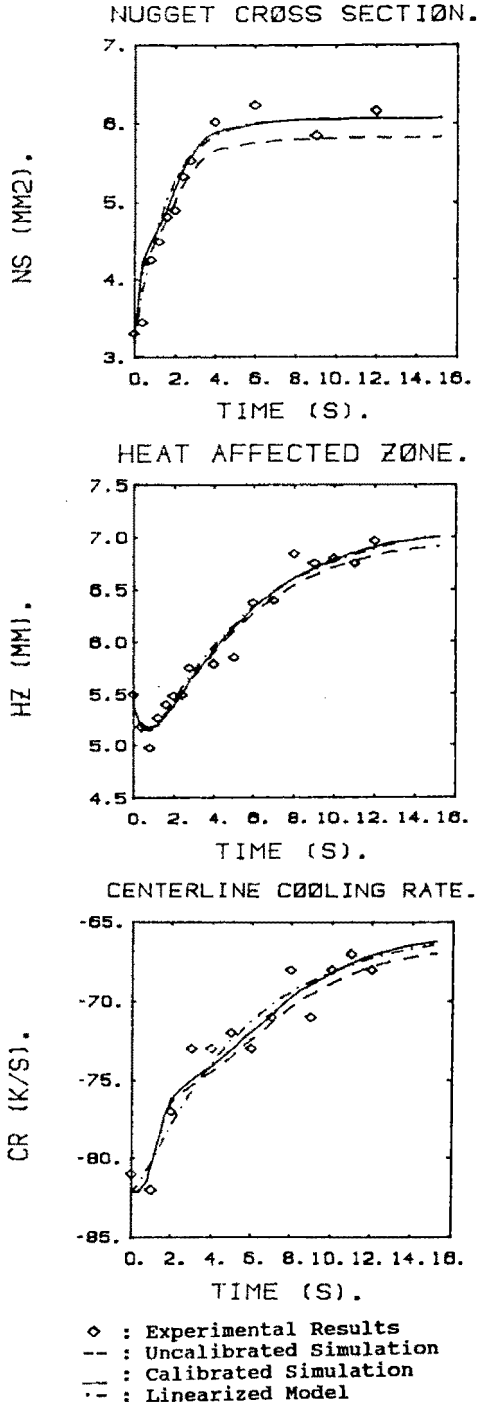

Fig. 7 Time responses of the outputs during a positive step to the heat input Q_1 (from $Q_1^* = 2500$ W to $1.2 \cdot Q_1^* = 3000$ W)

transfer functions match initial flat part of the nonlinear response. The calculated values of the gains and time constants of the linearized model are compiled in Table 1.

The table reveals the strong nonlinear dependence of the parameter values on the input magnitude. This is true even when compared to the experimentally determined repeatability of ±11 percent. Thus, Table 1 actually provides ranges of variation for the nonstationary model parameters and indicates the need for their in-process identification.

Finally, the linearized dependence of the welding outputs Y to the welding inputs U may be written in the form of a transfer matrix G as:

Table 1 Gains and time constants of the linearized dynamic model

Input \ Output		Nugget section NS (mm^2)		Heat affected zone HZ (mm)				Cooling rate CR (K/s)		
I	Step	K_a	τ_a	K_b	τ_b	τ_1	τ_2	K_c	τ_α	τ_β
Q_1	+0.2 Q_1^*	0.00574 mm^2/W	1.57 s	0.00356 mm/W	−1.56 s	5.42 s	0.50 s	0.0336 K/J	5.33 s	0.50 s
	−0.2 Q_1^*	0.00434 mm^2/W	0.63 s	0.00221 mm/W	−1.78 s	2.75 s	0.33 s	0.0632 K/J	4.43 s	0.61 s
v	+0.2 v^*	−0.91 mm.s	1.78 s	−1.21 s	−1.39 s	3.04 s	0.52 s	−27.9 K/mm	4.61 s	0.45 s
	−0.2 v^*	−1.12 mm.s	4.95 s	−3.40 s	−1.16 s	11.0 s	0.65 s	−25.5 K/mm	6.02 s	0.41 s
Q_2	+0.1 Q_1^*	0 mm^2/W	0 s	0.00051 mm/W	0 s	2.65 s	0 s	0.0976 K/J	2.40 s	0 s
	−0.1 Q_1^*	0 mm^2/W	0 s	0.00023 mm/W	0 s	2.41 s	0 s	0.1590 K/J	2.12 s	0 s

$$Y(s) = G(s) \cdot U(s) \tag{9}$$

with

$$Y(s) = \begin{bmatrix} NS(s) \\ HZ(s) \\ CR(s) \end{bmatrix}, \quad U(s) = \begin{bmatrix} Q_1(s) \\ v(s) \\ Q_2(s) \end{bmatrix}, \tag{10}$$

$$G(s) = \begin{bmatrix} NS/Q_1(s) & NS/v(s) & NS/Q_2(s) \\ HZ/Q_1(s) & HZ/v(s) & HZ/Q_2(s) \\ CR/Q_1(s) & CR/v(s) & CR/Q_2(s) \end{bmatrix}, \tag{11}$$

where all the elemental transfer functions of $G(s)$ are as given above. As already mentioned, the responses of the linearized outputs above to the same step inputs are indicated on Figs. 7–12 with a dot-dashed line.

9 Discussion

Despite the apparent success in capturing the system sequence in the form of nonstationary transfer functions, there are several important observations regarding the nature and cause of the observed responses.

First, during the transient to the nominal conditions of Fig. 6, the impulsive response of the cooling rate is because of the generation of a steep temperature hill at the beginning of welding. In particular, the positive excursion is caused by the initial heating the area directly under the torch, and it is soon followed by a sharp drop because of the high gradient of the newly developed temperature hill. These impulsive effects are not observable during the initiation of the secondary torch in Figs. 11 and 12 because CR is measured at the centerline location of the T_c isotherm of the already existing main torch temperature hill, at a point well behind the position of the secondary torch.

As already mentioned, the nonminimum phase character of the heat affected zone width response to steps in either Q_1 or v was expected, because of the definition of HZ as the difference between the widths of two different isotherms, namely T_h and T_m, each of which exhibits a quasi-first order response to steps of the above inputs. The time constant τ_2 of the pool isotherm T_m is less than the time constant τ_1 of the enveloping isotherm T_h of the HAZ, since the thermal time constant of the isotherms increases monotonically with decreasing isotherm temperature.

As explained in the derivation of the steady-state model, the cross-section of weld pool created by the secondary torch is not allowed to exceed that of the primary torch. Thus NS does not respond to small steps in Figs. 11 and 12. The small deviation observed in the heat affected zone width HZ from its nominal value during the steps in the secondary heat input Q_2 of Figs. 11 and 12 can actually be nullified by using a step of smaller size in Q_2, a longer distance x between the torches or for materials of smaller thermal diffusivity α such as stainless steel [10]. As already discussed, the optimization of the cooling rate for the double or N-torch configuration in Section 3 was based on this assumption of HZ being decoupled from the effect of Q_2, which greatly facilitates the design of a control strategy.

Finally, a closer look at the simulated responses of the cooling rate CR to steps of all three inputs reveals small-amplitude, high frequency oscillations superimposed to the dominant overdamped second order response, denoting the presence of complex conjugate pairs of poles far to the left of the dominant real poles. These contributions are insignificant in mild steel, but may become important in materials with smaller thermal diffusivity as was shown in [10] for stainless steel. There it was suspected that this oscillation stems from the periodic solidification of the material at the back of the pool (solidification front) in a variable rate, freeze-hold mode, to which the ripples of the weld bead are also attributed.

At this point it is possible to examine the agreement of the steady-state values of the welding outputs after the various steps in the welding inputs, with the steady-state model predictions of equation (2). To this end, the latter are equated to the corresponding experimentally obtained values, and the exponents n_a, n_b, n_c of the steady-state model expressions are calculated. These can be now compared to the respective expected values by the line and point source conduction models [15, 24] as follows:

(*a*) Nugget cross section NS: $n_a = 1.19$–1.51 (expected: $n_a = 1.25$)

(*b*) Heat affected zone HZ: $n_b = .936$–$.954$ (expected: $n_b = \ldots 1$)

(*c*) Center cooling rate CR: $n_c = 1.22$–1.38 (expected: $n_c = 1-2$)

This indicates that the nonlinear dependence of the steady-state values of the outputs NS, HZ, CR on the values of the inputs Q_1, v, Q_2 is in reasonable agreement with the predictions of the steady-state model. The small deviations are caused by the assumptions of the latter as well as its combination (during derivation) with empirical relationships formulated by different experimental data.

10 Conclusions

A set of welding outputs (the weld nugget cross section area, the heat affected zone width, and the centerline cooling rate) was selected to characterize the final microstructure and

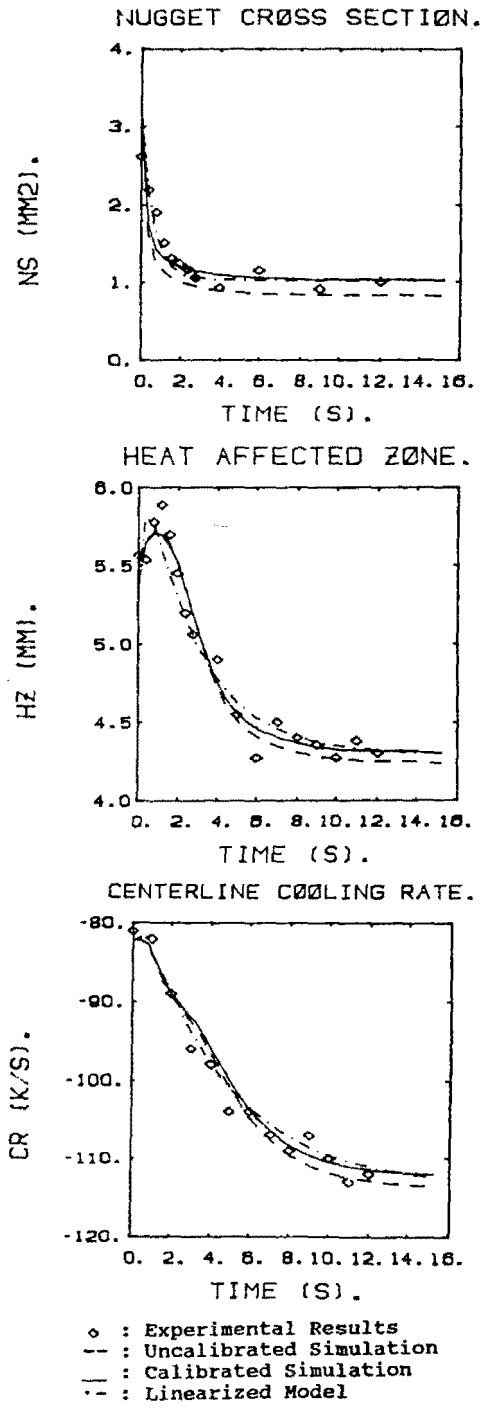

Fig. 8 Time responses of the outputs during a negative step to the heat input Q_1 (from $Q_1^* = 2500$ W to $0.8 \cdot Q_1^* = 2000$ W)

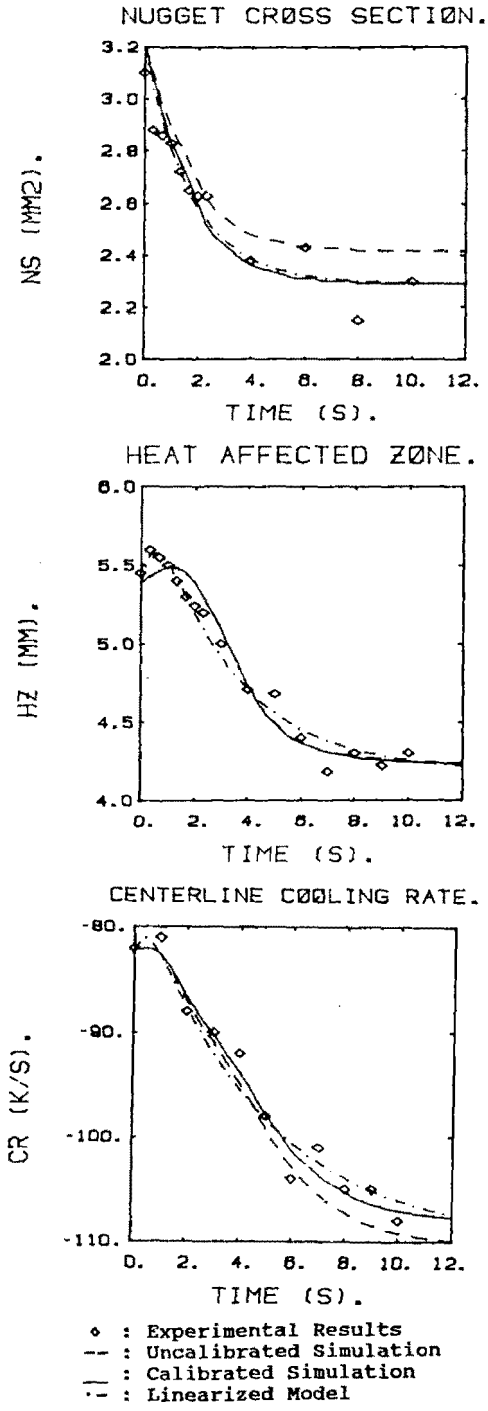

Fig. 9 Time responses of the outputs during a positive step to the torch velocity v (from $v^* = 5$ mm/s to $1.2 \cdot v^* = 6$ mm/s)

material properties of the weld joint, and a set of welding inputs (the heat input of main torch, travel speed, and the heat input of a secondary torch) was chosen as appropriate for the control of the outputs. A steady-state model as well as a finite difference numerical simulation were developed to describe the input-output dependencies, and their predictions were found to be in reasonable agreement to each other. After experimental calibration, the numerical simulation was validated as a dynamic model of the fusion welding process by comparing the simulated responses of the outputs NS, HZ, CR to step inputs in Q_1, v, Q_2 to experimentally observed transients. This dynamic model was then linearized in the neighborhood of an operating point and expressed in terms of low order transfer functions. The parameters of the resulting linear system, except for their dependence on the geometrical arrangement (plate thickness, torch distance), the material properties (thermal diffusivity) and the environmental conditions and process characteristics (arc efficiency, heat distribution, melt conduction), also depend on the values of the inputs because of the nonlinearity of the original dynamic model.

The purpose of this linearization was to facilitate the design of a thermal control system aiming at regulating the outputs NS, HZ and CR to a specified (or reference) set of values NS_d, HZ_d, and CR_d. These desired values will be experimentally

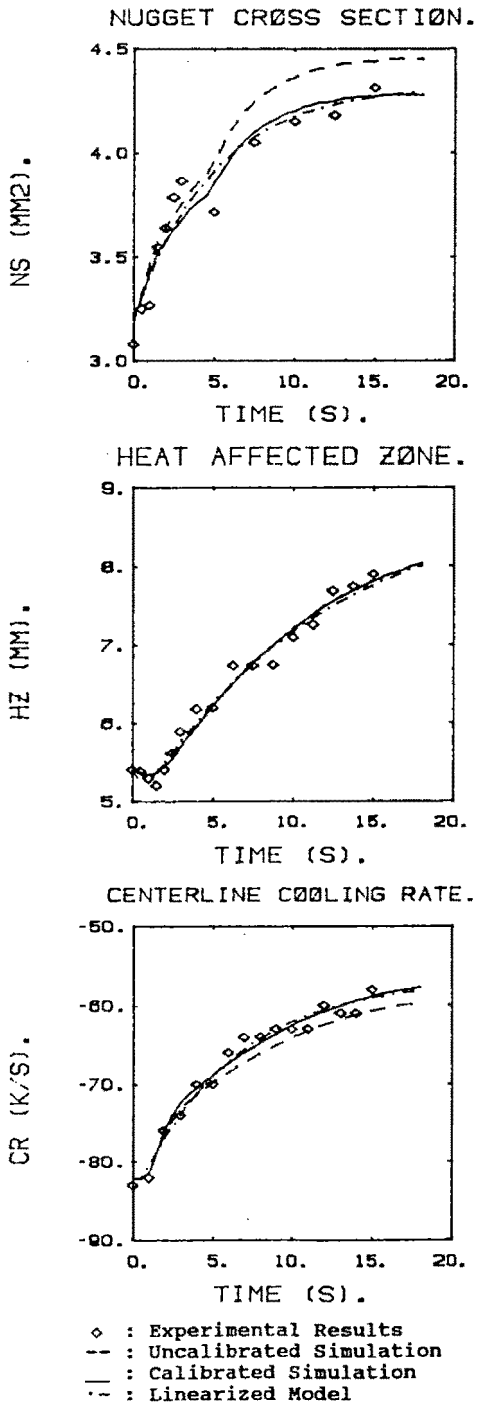

Fig. 10 Time responses of the outputs during a negative step to the torch velocity v (from $v^* = 5$ mm/s to $0.8 \cdot v^* = 4$ mm/s)

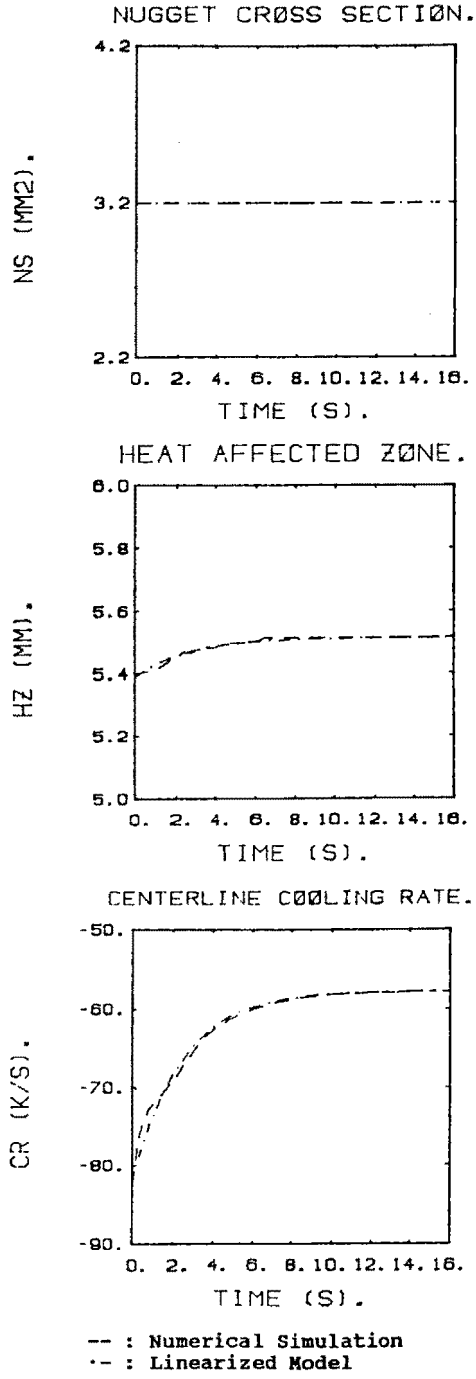

Fig. 11 Time responses of the outputs during a positive step to the secondary heat input Q_2 (from $Q_2^* = 0$ W to Qsrce = 250 W)

defined for each particular welding application so as to ensure consistently acceptable material microstructure distribution, and thus the desired material properties in the joint. The remaining steps to this purpose will include the implementation of an appropriate temperature sensor system and the design of a control scheme.

The necessary temperature sensing scheme for the evaluation of the outputs and the in-process identification of the model parameters will be based on the temperature measurements at distinct points of the top plate surface obtained by the infrared thermographic camera used in the modeling experiments before, interfaced to the computer controller [60-62]. As indicated by the hypothetical arrangement of Fig. 13, which illustrates the temperature measurement needs, the heat affected zone width HZ can be determined by appropriate interpolation of the T_h-isotherm among the measured temperatures at a number of lateral points. Similarly the centerline cooling rate can be determined by interpolation of the critical temperature T_c among the temperature measurements at a number of trailing points [10]. The estimation of the nugget cross section NS, which in the modeling experiments was directly (and destructively) measured off-line, normally requires the extrapolation of the T_m isotherm from the temperature measurements at the lateral top surface point and its interpolation among a number of measurements on the back center-line. The necessity for these measurements can be eliminated by a reliable correlation of the cross section area NS to optically measured values of the bead width and reinforcement height, and to ultrasonically measured values of

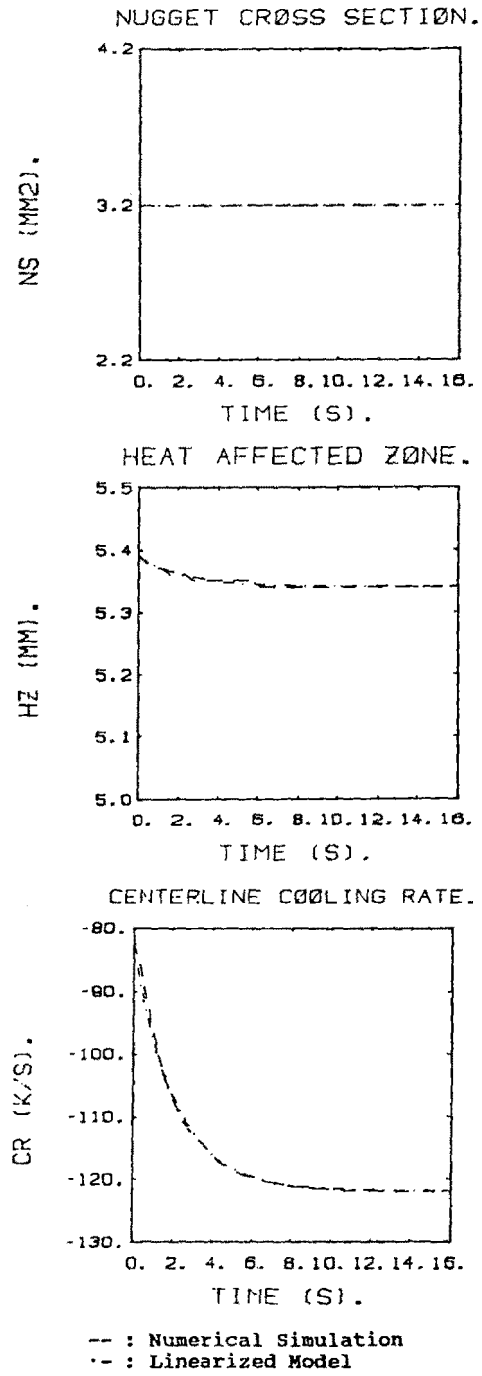

Fig. 12 Time responses of the outputs during a negative step to the secondary heat input Q_2 (from $Q_2^* = 0$ W to Qsink = −250W)

penetration [1, 63, 64], but the lack of direct measurement currently limits complete implementation of this scheme.

The intended multivariable closed-loop control system is illustrated in Fig. 14. Its design is based on the MIMO linearized model of the process, which, because of its input-output connection nature, does not provide state realizations with physically meaningful or directly observable states. The temperature measurements are used not only for the evaluation of the welding output values NS, HZ, CR, but also for the identification of the model parameters which tune the controller model. The need for this parameter adaptation stems from the dependence of the model parameters (gains and time constants for the linearized dynamic model) on the welding conditions as well as on the magnitude of the inputs. Thus, except for the nonlinear variation, the initial (structured) uncertainty and parameter drift during welding, the adaptation law is expected to handle abrupt changes in the welding geometry, process characteristics, environmental conditions and material properties. Moreover, the control law is required to ensure the robustness of the closed-loop system to unstructured uncertainty, i.e., tolerance to unmodeled dynamics of the welding process. Finally, the closed-loop system is expected to be asymptotically stable at least in the region of practical interest, and to show a satisfactory transient and steady-state performance. Various design approaches are possible under these control conditions, and the selection of the most efficient regulation scheme will depend on the particular circumstances and requirements, such as tracking of reference commands and rejection of disturbances of a specific nature and intensity.

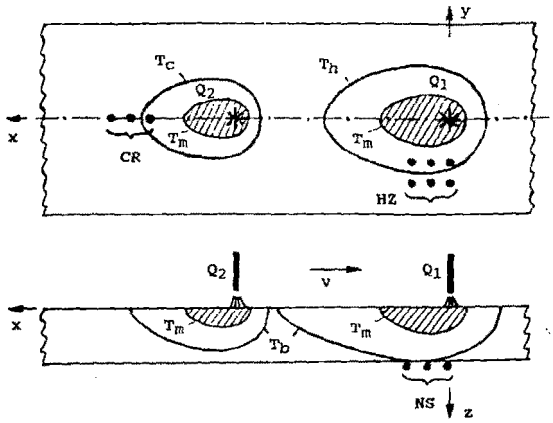

Fig. 13 The temperature measurement system

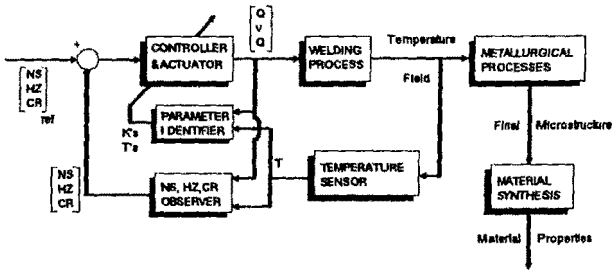

Fig. 14 The multivariable closed-loop control scheme

One such double-loop controller was recently developed in [65] on the basis of a discrete-time multivariable adaptive deadbeat algorithm. The parametrization of this controller was obtained by discretization of the above linearized model in an ARMA form, and the initial parameters were estimated using values from Table 1. The performance of the closed-loop system was simulated using the full numerical model as the plant. This indicated that good bandwidth can be obtained for simple parametrizations and short sampling periods (2 s). In actual implementation, such sample times were not possible because of actuator and thermal sensor speed limitations. A control system was finally implemented with a sample period of 2.4 s by redefining the outputs in a manner that allowed their rapid measurement and simplified the controller calculations. These modifications, and the details of the controller design will be the subject of a subsequent paper.

References

1 Boughton, P., Rider, G., and Smith, E. J., "Feedback of Weld Penetration in 1978," *Advances in Welding Processes*, Welding Institute 1978, pp. 203-209.

2 Vroman, A. R., and Brandt, H., "Feedback Control of GTA Welding Using Puddle Width Measurement," *Welding J.*, Sept. 1978, pp. 742-746.

3 Hunter, J. J., Bryce G. W., and Doherty, J., "On Line Control of the Arc Welding Process," *Developments in Mechanized, Automated and Robotic Welding*, Welding Institute 1980, pp. 37-49.

4 Hardt, D. E., Garlow, D. A., and Weinert, J. B., "A Model of Full Penetration Arc Welding for Control System Design," ASME JOURNAL OF DYNAMIC SYSTEMS, MEASUREMENT AND CONTROL, Vol. 107, Mar. 1985.

5 Dornfeld, D. A., Tomizuka, M., and Langari, G., "Modeling and Adaptive Control of Arc Welding Processes," *Measurement and Control for Batch Manufacturing*, Hardt Ed., Nov. 1982, pp. 65-75.

6 Cook, G. E., "Feedback and Adaptive Control to Process Variables in Arc Welding," *Developments in Mechanized, Automated and Robotic Welding*, Welding Institute 1980, pp. 321-329.

7 Linnert, G. E., et al., Arc Welding, *Metals Engineering Institute*, ASM 1968.

8 Udin, H., Funk, E. R., and Wulff, J., *Welding for Engineers*, Wiley, NY, 1967.

9 Masubuchi, K., *Analysis of Design and Fabrication of Welded Structures*, Pergamon Press, NY, 1980.

10 Doumanidis, C. C., "Real-Time Control of Thermal Properties in Welding," LMP Research Report LMP/FAR 86-05, MIT Jun. 1986.

11 Doumanidis, C. C., "A Survey of the Effects of Weld Imperfections on the Fracture Toughness of the Joint," unpubl. report, MIT 2301, 1986.

12 Doumanidis, C. C., M. Hale, and D. E. Hardt, "Multivariable Control of Arc Welding Processes," *Advances in Welding Science and Technology*, ASM International, 1986.

13 Carslaw, H. S., and Jaeger, J. C., *Conduction of Heat in Solids*, 2nd ed., Oxford Press, London, U.K., 1959.

14 Roberts, O. F. T., *Proc. Roy. Soc.* (A), Vol. 104, 1923, p. 640.

15 Rosenthal, D., "Mathematical Theory of Heat Distribution During Welding and Cutting," *Weld. J.*, Vol. 20, No. 5, 1941, pp. 220s-234s.

16 Rosenthal, D., Schmerber, R., "Thermal Study of Arc Welding: Experimental Verification of Theoretical Formulas," *Weld. J.*, Vol. 17, No. 2, 1938.

17 Rykalin, N. N., "The Calculation of Thermal Processes in Welding," Mashgiz 1951.

18 Wells, A. A., "Heat Flow in Welding," *Weld. J.*, Vol. 31, No. 5, 1952, pp. 263s-267s.

19 Roberts, D. K., and Wells, A. A., "A Mathematical Examination of the Effect of Bounding Planes on the Temperature Distribution due to Welding," *British Weld. J.*, Vol. 1, 1954, pp. 553-560.

20 Grosh, R. J., Trabant, E. A., "Arc Welding Temperatures," *Weld. J.*, Vol. 35, No. 8, 1956, pp. 396s-400s.

21 Adams, C. M., "Cooling Rates and Peak Temperatures in Fusion Welding," *Weld. J.*, Vol. 37, 1958, pp. 210s-215s.

22 Jhaveri, P., Moffatt, W. G., and Adams, C. M., "The Effect of Plate Thickness and Radiation on Heat Flow in Welding and Cutting," *Weld. J.*, Vol. 41, 1962, pp. 12s-16s.

23 Barry, J. M., Paley, Z., Adams, C. M., "Heat Conduction from Moving Arcs in Welding," *Weld. J.*, Vol. 42, 1962, pp. 97s-104s.

24 Myers, P. S., Uyehara, O. A., Borman, G. L., "Fundamentals of Heat Flow in Welding," *Weld. Res. Council Bulletin 123*, July 1967.

25 Kazimirov, A. A., Nedoseka, A. Y., and Sanchenko, V. A., "Calculating the Distribution of Heat During the Butt Welding of Plates Allowing for the Effect of Temperature on Physical Properties," *Autom. Welding* (USSR) Vol. 26, No. 11, Nov. 1973, pp. 30-32.

26 Kopersak, N. I., Slivinskii, A. M., and Dukhno, V. M., "Temperature Conditions in Weld Pools," *Autom. Weld.*, Vol. 7, 1973, pp. 1-3.

27 Malmuth, N. D., Hall, W. F., Davis, B. I., Rosen, C. D., "Transient Thermal Phenomena and Weld Geometry in GTA Welding," *Weld. J.*, Vol. 53, 1974, pp. 388s-400s.

28 Nedoseka, A. Y., Sanchenko, V. A., and Vorona, G. A., "Distribution of Temperature When a Concentrated Source of Heat Acts on the Surface of a Plate," *Autom. Weld.*, Vol. 30, No. 6, June 1977, pp. 1-4.

29 Willgoss, R. A., "Mathematical Model Predicts Equilibrium," *Welding & Metal Fabrication*, Vol. 52, No. 9, 1984, pp. 340-351.

30 Nunes, A. C., "An Extended Rosenthal Model," *Weld. J.*, June 1983, pp. 165s-170s.

31 Tsai, C. L., "Modeling of Thermal Behaviors of Metals During Welding," *Trends in Welding Research in the United States*, ASM, Metals Park, Ohio, pp. 77-89.

32 Mahla, E. M., Rowland, M. C., Shook, C. A., and Doan, G. E., "Heat Flow in Arc Welding," *Weld. J.*, Vol. 20, 1941, p. 459.

33 Jackson, C. E., and Shrubsall, A. E., "Energy Distribution in Electric Welding," *Weld. J.*, Vol. 29, No. 5, 1950, pp. 231s-241s.

34 Jackson, C. E., and Shrubsall, A. E., "Control of Penetration and Melting Ratio with Welding Technique," *Weld. J.*, Vol. 32, 1953, pp. 172s-178s.

35 Apps, R. L., Milner, D. R., "Heat Flow in Argon Arc Welding," *Brit. Weld. J.*, Oct. 1955, pp. 475-485.

36 Lesnewich, A., "Control of Melting Rate and Metal Transfer in Gas-Shielded Metal Arc Welding," *Weld. J.*, Vol. 37, No. 8, 1958, pp. 343s-353s and 418s-425s.

37 Cristensen, N., Davies, V. L., and Gjermundsen, K., "The Distributions of Temperatures in Arc Welding," *Brit. Weld. J.*, Vol. 12, Feb. 1965, pp. 54-75.

38 Bradstreet, B. J., "Effect of Welding Conditions on the Cooling Rate and Hardness in the Heat-Affected Zone," *Weld. J.*, Vol. 48, 1969, pp. 499s-504s.

39 Essers, W. G., and Walter, R., "Heat Transfer and Penetration Mechanisms with GMA and Plasma-GMA Welding," *Weld. J.*, Vol. 60, 1981, pp. 37s-42s.

40 Parshin, et al., "Algorithm for the Control of Dimensions of Welded Joints in Thin Sheets of High-Strength Steels," *Weld. Proc.* (USSR), Vol. 28, No. 10, Oct. 1981, pp. 3-6.

41 Thorn, K., Feenstra, M., Young, J. C., Lawson, W. H. S., and Kerr, H. W., "The Interaction of Process Variables—Their Influence on Weld Dimensions in GMA Welds on Steel Plates," *Metal Construction*, Vol. 14 No. 3, Mar. 1982, pp. 128-133.

42 Paschkis, V., "Estabilshment of Cooling Curves of Welds by Means of Electrical Analogy," *Weld. J.*, Vol. 22, 1943, p. 462.

43 Nippes, E. F., and Savage, W. F., "Development of Specimen Simulating Weld Heat Affected Zones," *Weld. J.*, Vol. 28, 1949, pp. 554-.

44 Makhnenko, V. I., Petun, L. A., Prilutskii, V. B., and Zamkov, V. M., "Assessing the Thermal Processes Taking Place Close to a Moving Weld Pool," *Autom. Weld.*, Vol. 22, No. 11, Nov. 1969, pp. 1-7.

45 Paley, Z., and Hibbert, P. D., "Computation of Temperatures in Actual Weld Designs," *Weld. J.*, Vol. 54, No. 11, 1975, pp. 385s-392s.

46 Kogan, M. G., Kryukovskii, V. N., and Pisarski, V. I., "The Temperature Field in the Weld Zone," *Autom. Weld.*, Vol. 32, No. 9, Sept. 1979, pp. 7-9.

47 Alberry, P. J., and Jones, W. K., "Computer Model for Prediction of HAZ Microstructures in Multi-pass Weldments," *Metal Technology*, Vol. 9, Oct. 1982, pp. 419-426.

48 Tall, L., "Residual Stresses in Welded Plates—A Theoretical Study," *Weld. J.*, Vol. 43, 1964, pp. 10s-23s.

49 Masubuchi, K., Simmons, F. B., Monroe, R. E., "Analysis of Thermal Stresses and Metal Movement During Welding," RSIC-820, Redstone Arsenal, Alabama, July 1969.

50 Hibbitt, H. D., and Marcal, P. V., "A Numerical Thermomechanical Model for the Welding and Subsequent Loading of a Fabricated Structure," *Computers and Structures*, Vol. 3, No. 5, Sept. 1973, pp. 1145-1174.

51 Friedman, E., "Thermomechanical Analysis of the Welding Process Using the Finite-Element Method," ASME *Journal of Pressure Vessel Technology*, Vol. 97, No. 3, Aug. 1975, pp. 206-213.

52 Doumanidis, C. C., "A Numerical Simulation of the Welding Process," LMP Research Report LMP/FAR 86-06, MIT, July 1986.

53 Giedt, W. H., Wei, X. C., and Wei, C. R., "Effect of Surface Convection Stationary GTA Weld Zone Temperatures," *Weld. J.*, Dec. 1984, pp. 376s-383s.

54 Boillot, J. P., Cielo, P., Begin, G., Michel, C., Lessard, M., Fafard, P., and Villemure, D., "Adaptive Welding by Fiber Optic Thermographic Sensing: An Analysis of Thermal and Instrumental Considerations," *Weld. J.*, July 1985, pp. 209s-217s.

55 Fitzpatrick, P. R., and Bah, M., "Thermal Analysis and Experimental Correlation of the TIG Welding Process," *Computer Technology in Welding 38*, The Welding Institute, London, U. K., 1986.

56 VDI Warmeatlas, "Berechnungsblatter fur den Warmeubergang" *VDI Verlag*, Dusseldorf, 1974, (Ed, Ga, Ka, Nb).

57 Automatix Inc., "RAIL Software Reference Manual for Robovision and Cybervision Systems," MN-RB-07, Billerica MA, Oct. 1983.

58 Inframetrics Inc., "Installation and Operation of the Inframetrics Model 600 IR Imaging Radiometer," 4625 Rev. B, Bedford, MA, Dec. 1985.

59 Thermoteknix Systems Ltd, "Operating Instructions for the Thermagram Thermal Image Processing System," Cambridge U.K., Jan. 1986.

60 Bennett, A. P., "The Interaction of Material Variability Upon Process Requirements in Automatic Welding," *Advances in Welding Processes*, WI, 1974.

61 Smith, C. J., "Self-Adaptive Control of Penetration in Tungsten Inert Gas Weld," *Adv. Weld.* Proc, WI, 1978.

62 Nomura, H., et al., "Arc Light Intensity Control Current in SA Welding System," *Journal of Welding and Metal Fabrication*, Sept. 1980.

63 Richardson, R. W., Gutow, D. A., and Rao, S. H., "A Vision-Based System for Weld Pool Size Control," *Measurement and Control for Batch Manufacturing*, Hardt Ed, Nov. 1982, pp. 65-75.

64 Hardt, D. E., and Katz, J., "Ultrasonic Measurement of Weld Penetration," *Weld. J.*, Sept. 1984, pp. 273s-278s.

65 Doumanidis, C. C., "Modeling and Control of Thermal Phenomena in Welding," Ph.D. thesis, Dept. of ME, MIT, Jan. 1988.